Engineering Structures 48 (2013) 750–762

Contents lists available at SciVerse ScienceDirect

Engineering Structures

journal homepage: www.elsevier.com/locate/engstruct

Experimental study on cyclic behavior of trapezoidally corrugated steel shear walls

Fereshteh Emami, Massood Mofid *, Abolhassan Vafai

Center of Excellence in Structures and Earthquake Engineering, Civil Engineering Department, Sharif University of Technology, Tehran, Iran

ARTICLE INFO

Article history:
Received 28 November 2011
Revised 10 November 2012
Accepted 13 November 2012
Available online 10 January 2013

Keywords:
Corrugated steel shear wall
Buckling
Energy dissipation
Ductility
Cyclic loading

ABSTRACT

This paper presents the research works on the cyclic behavior of trapezoidally corrugated as well as unstiffened steel shear walls. A series of experimental studies were carried out on the half-scale, one-story, single-bay steel shear walls with unstiffened and trapezoidally corrugated panels. This experimental study was conducted to compare the stiffness, strength, ductility ratio and energy dissipation capacity of three different steel shear walls: unstiffened, trapezoidally vertical corrugated and trapezoidally horizontal corrugated. Gravity loads were not applied at the top of the walls and horizontal load was applied at the top of each specimen. Loading sequence was applied as displacement-control with increasing and decreasing amplitudes. The results reveal that although the ultimate strength of the unstiffened specimen is nearly 17% larger compared to that of the corrugated specimens, energy dissipation capacity, ductility ratio and the initial stiffness of the corrugated specimens are approximately 52%, 40% and 20% larger compared to the unstiffened specimen, respectively. The existing methods of analyzing unstiffened steel shear walls were also employed to evaluate the corrugated specimens. Although fairly good correlations were found between experimental and analytical studies in the initial stiffness and ultimate strength, more studies need to be implemented.

1. Introduction

Steel structures have been widely utilized in the building constructions in seismic hazard area due to their higher strength and ductility. Lateral load-resisting systems in steel buildings are usually designed as the moment resisting frames or braced frames. There are advantages and disadvantages for each system. For instance, the ductility of the moment frames is usually higher than that of the braced frames and the stiffness of the braced frames is usually higher than that of the moment frames. However, the construction cost of the braced frames is higher. The steel shear wall is another possible option as a lateral resisting system where it is appropriate for either a new structure or as a means to retrofit an existing building. This system consists of steel plates, one story high and one bay wide connected to the adjacent beams and columns by weld, bolt or both. The plates are installed in one or more bays for the full height of the building. The surrounding steel frame can be applied with either simple or moment-resisting beam-to-column connections. A properly designed steel shear wall has very ductile behavior and relatively large energy dissipation capacity. Furthermore, the steel shear wall as an efficient and economical lateral load resisting option has high initial stiffness and is highly effective in limiting the lateral drift of structures. When moment-resisting beam-to-column connections are present in this system, it has inherent redundancy and significant energy dissipation [1].

Numerous researches on the steel shear wall have been conducted. The experimental studies on the thin steel shear walls have been performed under cyclic loading [1–3]. Moreover, the analytical studies on the shear buckling characteristics and behavior of the multi-story thin steel shear wall have also been conducted [4–11]. Shear buckling behavior of the steel plate is the main concern of the thin steel plate shear wall. The buckling behavior of the shear panel can transform from global to local or interactive buckling by adding stiffeners. Therefore, the steel shear wall is applied in two types, stiffened and unstiffened. The stiffened type has higher stiffness and strength. Furthermore, stiffening the panel can heavily increase the amount of energy dissipated under cyclic loading [12]. However, in the stiffened system, the construction cost is considerably higher. The most important reason for higher construction cost is due to its time-consuming factor and the high cost of thin plates welding. To design the stiffened and unstiffened steel shear walls, two methods are employed: strip model and Plate-Frame Interaction (PFI). Postbuckling strength of the panel has been considered in both models [8,13]. Since construction cost of stiffened panels is immensely high, corrugated shear panel is proposed as an innovative lateral resisting system in this research.

* Corresponding author. Tel./fax: +98 2166014828.
E-mail addresses: sf_emami@yahoo.com (F. Emami), mofid@sharif.edu (M. Mofid), Vafai@sharif.edu (A. Vafai).

0141-0296/$ - see front matter © 2012 Elsevier Ltd. All rights reserved.
http://dx.doi.org/10.1016/j.engstruct.2012.11.028

In this experimental study, trapezoidally corrugated steel shear wall is investigated as a new option. This type of steel shear wall has larger buckling strength due to out-of-plane stiffness. Presently, trapezoidally corrugated plates are utilized as web of plate girders. Their shear buckling strength is described as interactive shear buckling. The research on the shear buckling behavior of the corrugated plates has been initiated by Easley and McFarland [14]. Afterwards, numerical and experimental studies on the buckling behavior and strength of the corrugated webs have been conducted by Elgaaly et al. [15,16], Sayed-Ahmed [17] and Yi et al. [18]. Despite the significant research, the shear buckling characteristic of the trapezoidally corrugated webs has not been clearly explained. However, the value of the interactive shear buckling is affected by global, local and yield stress of the corrugated webs.

Totally, the corrugated steel shear walls are considered as improved option due to the following reasons such as local or interactive buckling in return of global buckling, more initial stiffness, more out-of-plane stiffness, lower construction cost and accordion behavior of corrugated panels. Thus, this paper describes the cyclic testing of a series of one story; half scale trapezoidally corrugated steel shear walls. In this experimental research, cyclic load was exerted on the two models of the half scale corrugated steel shear walls as well as one model of the half scale unstiffened steel shear wall. All models were similar in thickness and specification of boundary frames as well as their connections. In order to initiate the simulation of the steel shear walls as in the real world practice, no special or unusual fabrication techniques were employed. All specimens were fixed at the bottom and had moment-resisting beam-to-column connections. The tests were conducted according to an approved method for the simulation of seismic loads [19]. Besides, gravity loads were not applied for any specimens. A series of analytical studies were also conducted to examine elastic and inelastic behavior of the corrugated steel shear walls.

2. Experimental program

2.1. Specimen types

Totally, three specimens were designed and constructed to investigate and distinguish the cyclic behavior of the trapezoidally vertical and horizontal corrugated steel shear walls with unstiffened steel shear wall. All the specimens were constructed in half-scale, one-story and single-bay. The first specimen was an unstiffened steel shear wall which was designed based on PFI method [8]. According to the PFI method, the strength of an unstiffened steel shear wall is the sum of the shear panel strength and its surrounding frame strength. The ultimate strength (F_{wu}) and limiting shear elastic displacement (U_{we}) of the shear panel are calculated as follows:

$$F_{wu} = Lt(\tau_{cr} + (1/2)\sigma_{ty}\sin 2\theta) \tag{1}$$

$$U_{we} = U_{wcr} + U_{wpb} \tag{2}$$

As known, in thin plates, tension field action configures after plate buckling. In fact, post-buckling strength of the thin plates is highly significant. In Eq. (1), L and t are width and thickness of panel, respectively. τ_{cr} is critical shear stress, σ_{ty} is tension field stress corresponding to the panel yield obtained based on the Von-Mises yield criterion and θ is inclination angle of the tension field measured relative to horizontal axis. In Eq. (2), U_{we} is the sum of shear buckling displacement of the panel (U_{wcr}) and shear displacement of the panel due to the configuration of the tension field (U_{wpb}). U_{wpb} is calculated with the conception of equality of work performed by shear stresses and strain energy as:

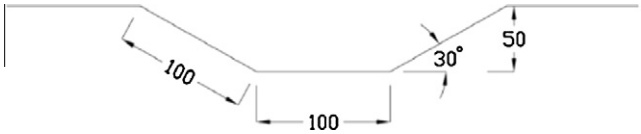

Fig. 1. Geometric properties of trapezoidally corrugated plate (mm).

$$\frac{1}{2}\left[(\frac{1}{2}\sigma_{ty}\sin 2\theta)tL\right]U_{wpb} = \iiint F_0 dxdydz \tag{3}$$

where $F_0 = \frac{1}{2}\left[\frac{1+\nu}{E}\left(\sigma_{xx}^2+\sigma_{yy}^2+\sigma_{zz}^2\right) - \frac{\nu}{E}(\sigma_{xx}+\sigma_{yy}+\sigma_{zz})^2 + \frac{2(1+\nu)}{E}\left(\sigma_{xy}^2+\sigma_{xz}^2+\sigma_{yz}^2\right)\right]$. Finally, U_{we} is obtained as follows:

$$U_{we} = (\tau_{cr}/G + 2\sigma_{ty}/E\sin 2\theta)h_s \tag{4}$$

σ_{ij} (i and $j = x, y$ or z) are stress components; ν, E and G are Poisson's ratio, Young's modulus of elasticity and Shear modulus of elesticity, respectively. According to the PFI method, the ultimate shear force of the surrounding frame is calculated as:

$$F_{fu} = 4M_{fp}/h_s \tag{5}$$

$$U_{fe} = M_{fp}.h_s^2/6EI_f \tag{6}$$

where M_{fp} and I_f are plastic moment capacity and moment inertia of the column, respectively and h_s is height of the panel. For monotonous distribution of the tension field action, it is required that the columns and top beam to be adequately rigid. This is attained through controlling the following relations:

$$M_{fp} > (\sigma_{ty}th_s^2/4)\cos^2\theta \tag{7}$$

$$M_{sp} > (\sigma_{ty}th_s^2/8)\sin^2\theta \tag{8}$$

where M_{sp} is plastic moment capacity of the beam. To design the first specimen, by applying Eqs. (1), (4), (5), and (6), the amount of F_{wu}, U_{we}, F_{fu} and U_{fe} were calculated and then relations (7) and (8) were considered. Furthermore, the amount of inclination angle of the tension field measured relative to horizontal axis (θ) assumed to be 45°.

The second specimen was the trapezoidally vertical corrugated and the third specimen was the trapezoidally horizontal corrugated steel shear wall. Boundary frames in the corrugated specimens were considered to be similar to that of the first specimen in order to provide the opportunity to compare the seismic behavior of the specimens. Furthermore, the applied shear plates in all the specimens were similar in both panel thickness and mechanical properties; however, they just turned into the trapezoidal form for the corrugated specimens. Geometric properties of the corrugated panels are shown in Fig. 1.

The details of the tested specimens are shown in Figs. 2–4. In each specimen, the top beam section is HE-B140 and the section of columns is HE-B160. The bottom beam section in each specimen is HE-B200 which is connected to strong floor beam of laboratory by M24 bolts. HE-B is I-shape wide flange according to the European Standard, equivalent to IPB. The dimensions of the panel in each specimen are 1480 × 1980 with thickness of 1.25 mm. The summary of design specimens is listed in Table 1.

2.2. Material properties

Mechanical properties of the steel plates and the steel profiles applied in the construction of the specimens are reported in Table 2. The mechanical properties were determined by coupon test performed according to the ASTM E8M-04 [20]. The values obtained by the coupon test indicate that the shear panel is St12 steel and the boundary frames are St44 steel according to the DIN Standard

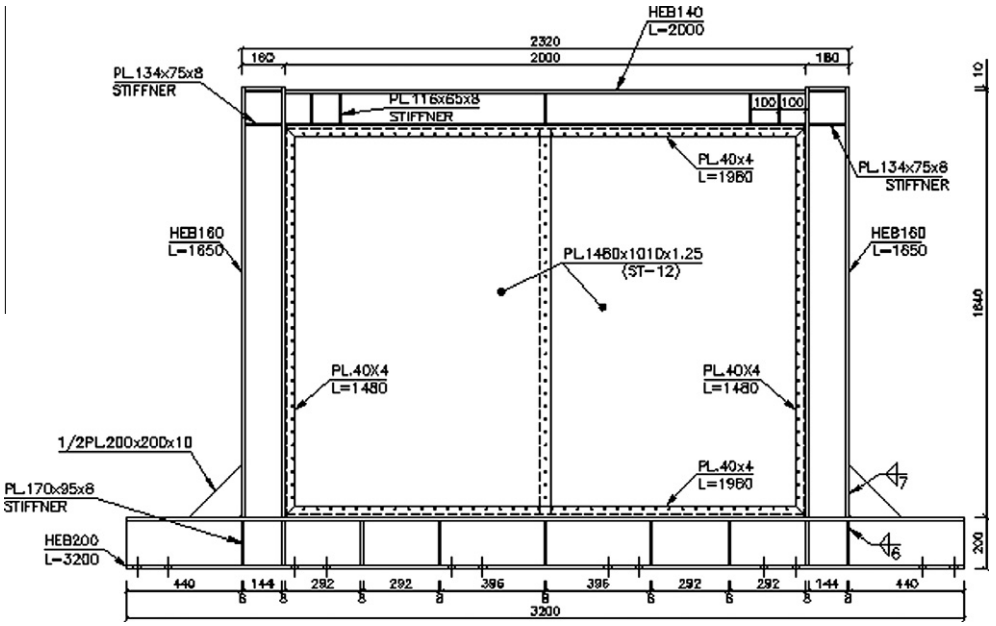

Fig. 2. Specimen no. 1 (mm).

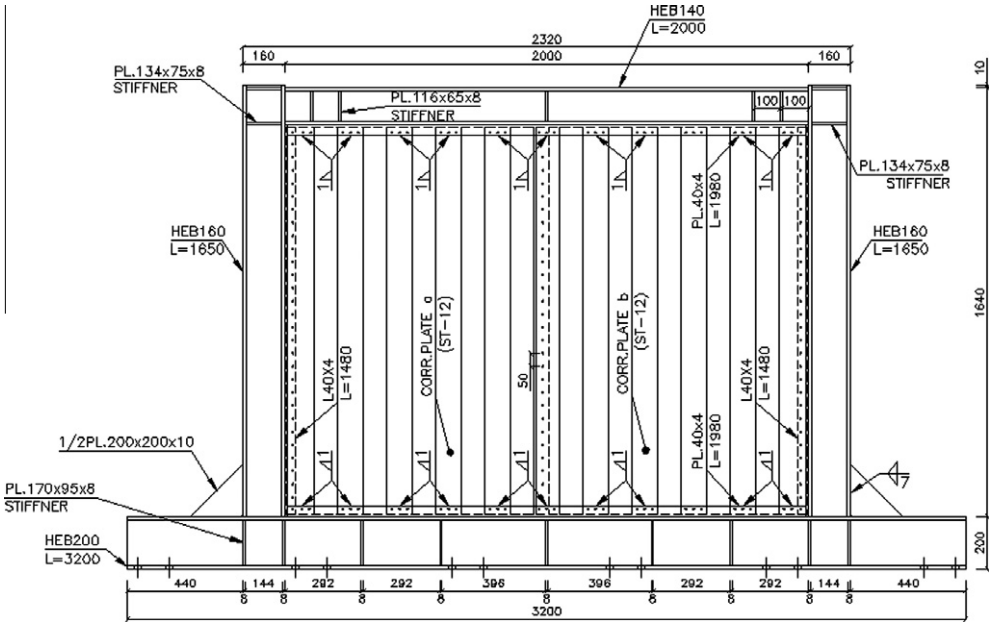

Fig. 3. Specimen no. 2 (mm).

[21]. By a proper design, this steel panel is able to yield at a predetermined force level and dissipates the seismic energy via plastic deformation. Therefore, steel shear wall does carry ample post-yield stiffness until it reaches its ultimate strength. The lower yield strength of panel provides better distribution of strength rate between the shear panel and its surrounding members as well. Furthermore, it ultimately ensures that the frame would not collapse before the wall reaches its ultimate strength.

2.3. Test setup

As it was formerly described, each specimen was connected to the strong floor beam of the laboratory by fastening bottom flange of its bottom beam. The test setup of specimen nos. 1–3 is shown in Fig. 5. The connection of each column to the bottom beam was developed utilizing complete penetration groove welds of its flanges and fillet weld of its web, i.e., this connection was fully moment-resisting. The connection of the top beam to the columns was moment-resisting as well, i.e., complete penetration groove welds of beam flanges and fillet welds of beam web to the columns were used. After construction of the specimens, quality control of the welds was tested. Ultrasonic testing for groove welds and penetration testing for fillet weld were performed based on the AWS standard [22]. In order to prevent the out of plane movement, two beams were applied as lateral supports in top level of each specimen in both sides. The shear panel was connected to the surrounding frames by fish plates. Fish plate-to-shear panel connection was simultaneously performed by welds and bolts. Despite

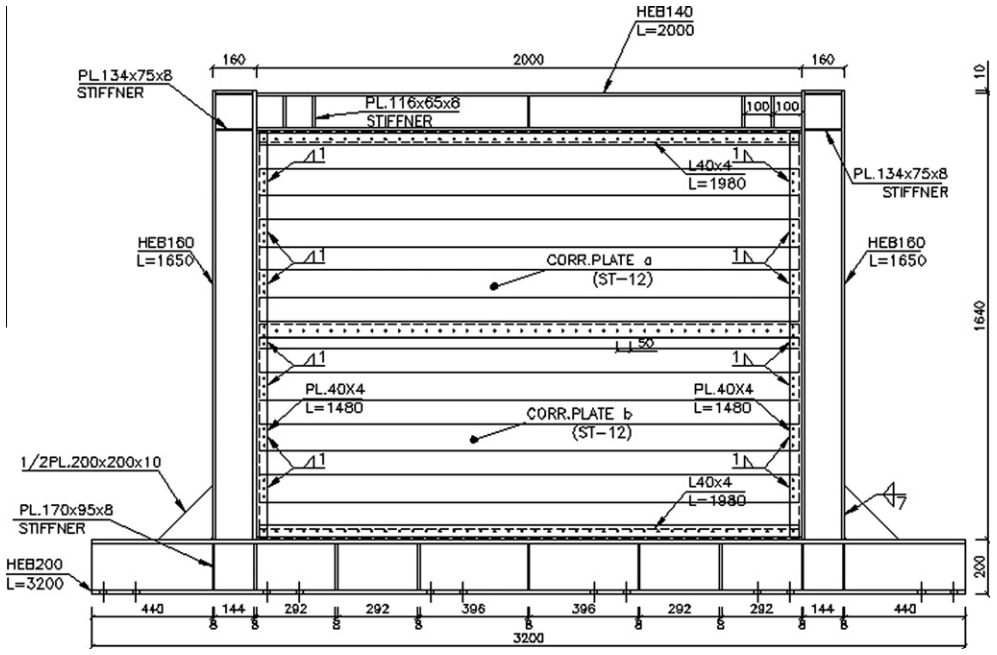

Fig. 4. Specimen no. 3 (mm).

Table 1
Design of specimens (unit: mm).

Specimens	Beam	Column	Plate thickness	L/t	h_s/t	Type panel
No. 1	HE-B140	HE-B160	1.25	1600	1200	Unstiffened
No. 2	HE-B140	HE-B160	1.25	1600	1200	Vertical corrugated
No. 3	HE-B140	HE-B160	1.25	1600	1200	Horizontal corrugated

Table 2
Mechanical properties.

Type	Young's modulus E (GPa)	Yield stress f_y (MPa)	Ultimate stress f_u (MPa)	f_y/f_u	Percent elongation (%)
Plate	210	207	290	0.71	41
Column	210	300	443	0.67	33
Beam	210	288	456	0.63	37

the fact that quality control of the welds was tested, there was a possibility of weld defection duo to the thin thickness of the infill shear panels. Besides, effective thickness of the welds applied for the connection of the shear panel to the fish plate or angle was 1 mm whereas the shear panel thickness was 1.25 mm. Therefore, hybrid connection (combination of weld and bolt) was utilized to prevent creating failure in the connection. In fact, considering the ultimate tension strength of the shear panel, A325 bolts were applied and accompanied with the fillet welds in its connection area to the fish plate. This means connection strength is the sum of the strength of the welds and bolts. Due to the limitations in dimensions of the produced thin steel plates, one splice was situated in mid-span of the shear panel in any specimen. For example, splice detail and panel-to-beam connection of the specimen no. 1 as well as details of corrugated panel-to-beam and column connections of the specimen no. 3 are shown in Fig. 6. Each specimen was connected to the girder of strong floor by M24 bolts. The arrangement of bolts and their details is illustrated in Fig. 7.

2.4. Loading program and measurements

To simulate earthquake load and further to investigate the cyclic behavior, quasi-static cyclic tests are employed which use a horizontal in-plane load history; moreover, they use gradual increasing loads or displacements in successive cycles [23]. As far as most earthquakes are concerned, the maximum accelerations and deformations occur in early seconds of events; furthermore, amplitude of displacements has an increasing and decaying sequence. Therefore, AC154 protocol was applied in order to obtain a more logical evaluation of the cyclic behavior. This protocol provides the acceptance criteria for cyclic racking shear tests for metal sheeted shear walls. According to the AC154, the racking shear loads will be applied at the top of the wall assembly in accordance with the sequential phased displacements. In addition, the load frequency utilized in the test will be in the range of 0.2–1.0 cycles per second [19]. In this study, due to the limited equipment in the laboratory, the hydraulic jacks applied the cyclic load where they were controlled by the laboratory technicians. Therefore, the load frequency was not controlled automatically, and consequently load sequence is somewhat an approximate value.

Based on the AC154, displacements will be continuously measured using displacement transducers having a minimum resolution of 0.13 mm. Based on this instruction, Approximate Elastic Displacement (AED) is determined using a monotonic or cyclic test. In the cyclic test, a value of 20.3 mm can be assumed for the AED to establish the AED for other tests. This instruction describes the number of loading cycles and the maximum horizontal displacement applied at the top of wall as the following:

- The loading procedure consists of the first three cycles applied as fully-reversing displacement increment representing 25%, 50% and 75% of the AED.
- Top wall displacement is then increased to 100% of the AED for one cycle.

Fig. 5. Setup of specimens.

- Next, decay cycles of displacement consisting of only one cycle with 75%, 50% and 25% of the AED, respectively.
- Followed by three cycles of displacement at 100% AED to stabilize the force–displacement response.
- The next increment of increased displacement (125% of AED) is then applied, followed by similar decay and stabilization cycles.
- The increment force–displacement and decay cycles will be continued to 150%, 175%, 200%, 250%, 300% 350% and 400% of the AED or until the applied force diminishes to 25% of the maximum strength. The described procedure of cyclic loading is shown in Fig. 8.

In this experimental research, because of the limitation in the number of specimens and further in order to establish the possibility of a more precise comparison of cyclic behavior of the three specimens, the approximate value of 20 mm was utilized as the value of the AED. However, for more accurate evaluation of the buckling and the initial elastic behavior of each specimen, the initial displacement cycles were begun with amplitude lower than 25% of the AED and each displacement amplitude was repeated two cycles in return of three cycles. Since then, loading was continued according to the instruction. As it was described, in this study, loading was conducted as displacement controlled and gravity loads were not applied. During loading by load cell, the value of the exerted load and the amount of displacement at the top of the specimens were continuously measured. Besides, the displacement transducers measured the amount of deformation in the other positions of the specimens where all of the measurements were recorded by data logger. The amount of strain measured by both axial and triaxial strain gauges was simultaneously recorded by data logger. The location of the strain gauges is indicated in Fig. 9.

3. Experimental results

The variations of stiffness, energy dissipation capacity, ductility and ultimate strength are the main characteristics which affect the seismic performance of the steel shear wall. In this experimental research, for each specimen, loading was stopped when the value of the wall strength decreased relative to the ultimate strength with increasing displacement amplitude, or when displacement amplitude reached 100 mm. Hysteretic behaviors of all the specimens are shown in Fig. 10. Further, Fig. 11 indicates the typical deformation pattern after the structural testing. Although hysteretic behavior of the unstiffened and corrugated specimens along with their load distribution pattern was different, eventually all the specimens failed after significant inelastic tension field action occurred with a large story drift deformation. In addition, in both corrugated specimens unlike the unstiffened specimen, the total capacity of the panel was utilized so that yielding and tearing were observed in most of the shear panel positions. The following are the discussions of the experimental loading.

3.1. Specimens' behavior during loading

3.1.1. Specimen no. 1

Elastic buckling of the infill shear panel was observed during cycle 1 (with drift 1 mm). Yielding primarily occurred during cycle 2 (the first cycle with drift 3 mm) in the bottom right corner of the infill shear panel. By increasing load and displacement amplitude, the yielded areas on the infill shear panel grew larger. In cycles 6 and 8 (with drifts 10 and 15 mm), plastic hinge created in the beam and column, respectively. With increasing displacement amplitude in the subsequent cycles, the infill shear panel buckled at the maximum displacement accompanied with several loud bangs. These noises occurred in each cycle as the panel buckles popped through and reoriented themselves upon reversal of the loading direction.

The first tear was detected during cycle 23 (the third cycle with drift 25 mm) in the left top corner of the infill panel. It was 4 mm long and located near the weld connecting the infill panel to the fish plate. By cycles 28 and 38 (with drifts 30 and 40 mm), the second and third tears were detected near the splice of the infill panel and in the right top corner of the infill panel, respectively. By continuing the loading, column flange distortion as well as beam-column connection distortion formed and progressed gradually. Furthermore, the dimension of the tears of the infill panel increased. Finally, in cycle 50 (with drift 70 mm); the shear force reached approximately 580 KN. Subsequently, shear force decreased with increasing displacement amplitude. By cycle 54, the

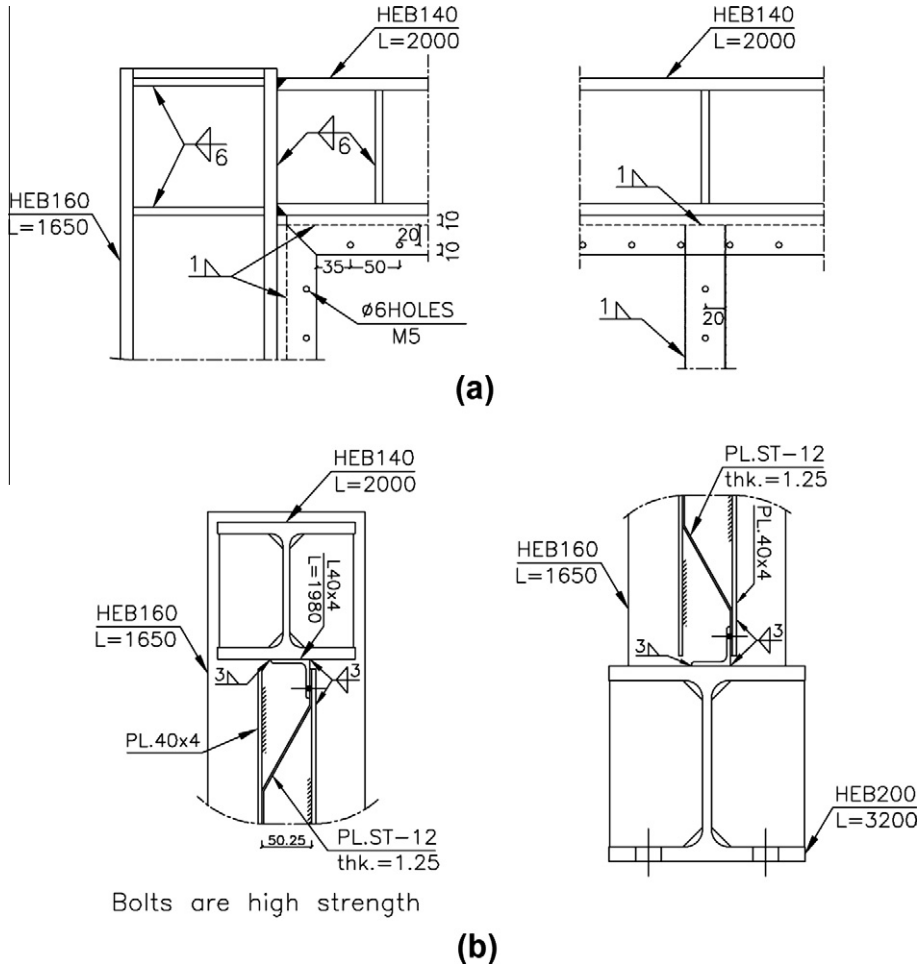

Fig. 6. Connection details: (a) beam-to-column connection and detail of splice in specimen no. 1; (b) connection of corrugated panel to column in specimen no. 3.

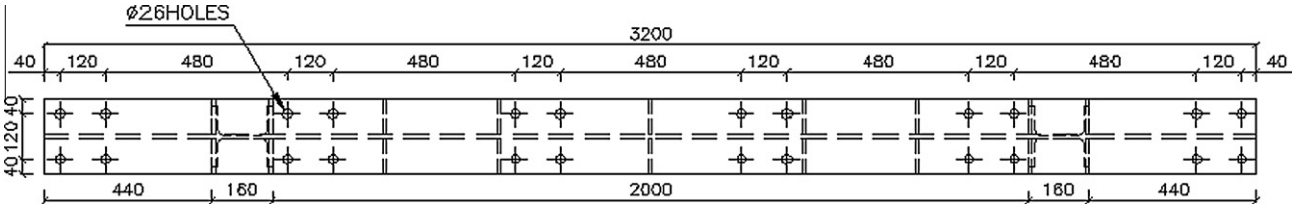

Fig. 7. Detail of connection of bottom beam to strong floor girder.

stiffener of the right column in the location of the beam-column connection was cut out and the loading was terminated.

3.1.2. Specimen no. 2

Buckling of the infill shear panel was observed during cycle 2 (with drift 3 mm). These observed deformations in the corrugated panel unlike the specimen no. 1 were local and occurred primarily in the right bottom corner of the infill panel. In addition, yielding first occurred during cycle 2 (the first cycle with drift 3 mm) near the left bottom corner of the infill shear panel. By increasing load and displacement amplitude, the yielded areas on the infill shear panel grew larger. By continuing the loading (with increasing displacement amplitude), most deformations occurred in the bottom of the infill panel and developed upward the infill panel gradually. Furthermore, noises created due to the deformation of the infill panel were much less than the specimen no. 1. During cycle 10 (with drift 20 mm), plastic hinge created in the beam and column, respectively.

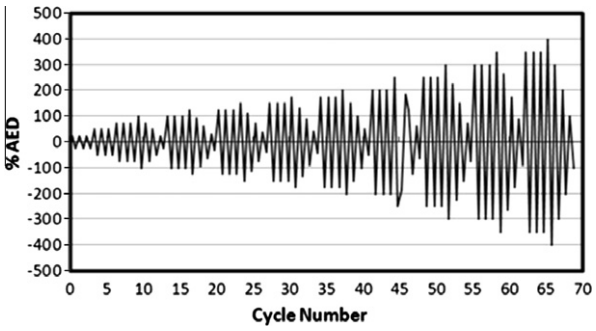

Fig. 8. Quasi-static displacement control loading sequence.

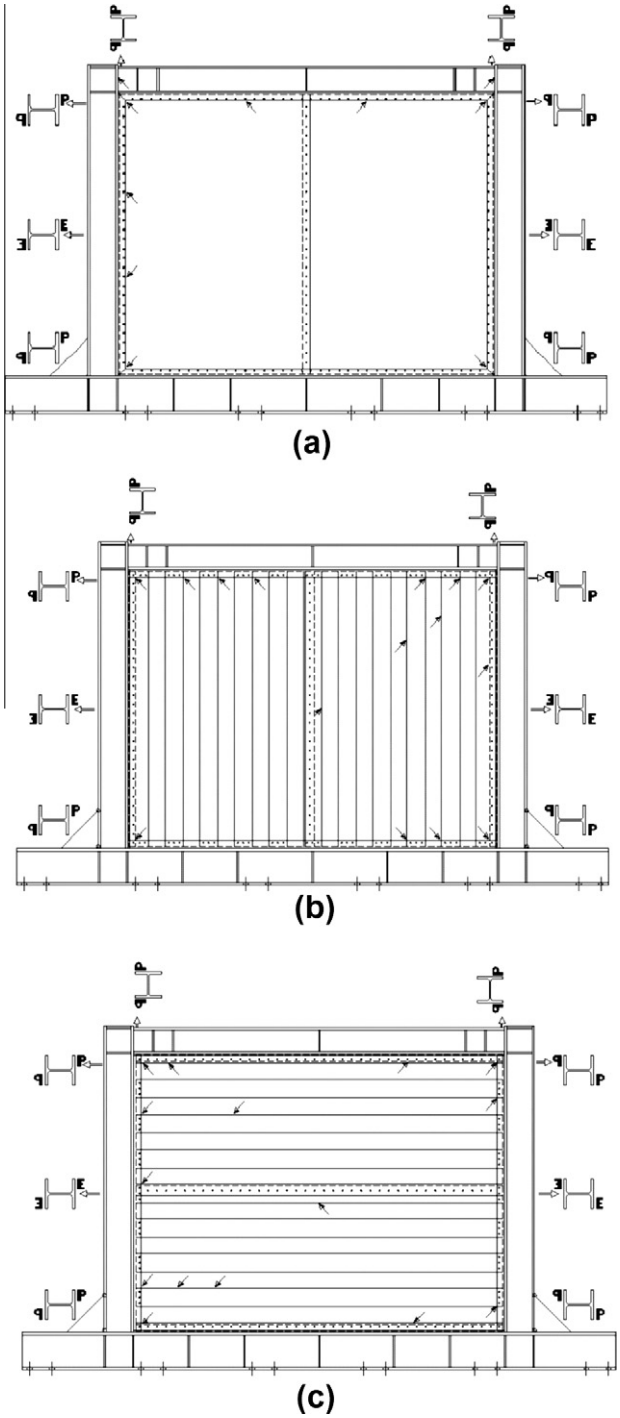

Fig. 9. Location of strain gauges: (a) specimen no. 1; (b) specimen no. 2; (c) specimen no. 3.

The first tear was detected during cycle 13 (the second cycle with drift 20 mm) in the left bottom part of the infill panel. It was 2 mm long and located at the distance of 660 mm from the left column and 300 mm from the bottom of the infill panel. By cycles 15 and 16, the second and third tears were detected near the splice of the infill panel and in the right bottom part of the infill panel, respectively. By continuing the loading, one or two tears were added to the infill panel tears in each cycle. In fact, in this specimen unlike the specimen no. 1, the number of tears was successively increased whereas dimension of them was gradually developed. Furthermore, inclination angle of the tension field measured from the horizontal axis was approximately 60° in this specimen.

By continuing the loading, welds connecting the infill panel to the fish plates located on the bottom beam were cut out and bolts were either thrown out or cut out as well. Finally, in cycle 54 (with drift 100 mm), shear force was 500 KN. Afterwards, displacement amplitude was decreased and the loading was terminated.

3.1.3. Specimen no. 3

Buckling of the infill shear panel was observed during cycle 2 (with drift 3 mm). These observed deformations in this corrugated panel unlike the specimen no. 1 were local which included four parts of the corrugations and the first occurred in the right top part of the infill panel. Yielding occurred primarily during cycle 2 (the first cycle with drift 3 mm) near the left corner of the bottom infill shear panel. By increasing load and displacement amplitude, the yielded areas on the infill shear panel grew larger. With increasing displacement amplitude, the tension field created between columns so that inclination angle of the tension field measured from the horizontal axis was approximately 30°. Furthermore, noises created due to the deformation of the infill panel were similar to the specimen no. 2. During cycles 7 and 10 (with drifts 15 and 20 mm), plastic hinge created in the beam and column, respectively.

The first tear was detected during cycle 12 (the first cycle with drift 20 mm) in the right top part of the infill panel. It was 3 mm long and located at the distance of 500 mm from the right column and 420 mm from the top of the infill panel. By cycle 20, the second and third tears were detected; one near the splice of the infill panel at the distance of 400 mm from the left column and the other in the amid of top part of the infill panel at the distance of 320 mm from the top of the infill panel. By continuing the loading, one or two tears were added to the infill panel tears, in each cycle. In fact, in this specimen similar to the specimen no. 2, number of tears was successively increased whereas dimension of them was gradually developed.

By continuing the loading, welds connecting the infill panel to the fish plates located on the columns were being cut out and also their bolts were being either thrown out or cut out. Finally, in cycle 57 (with drift 90 mm); shear force achieved to 490 KN. In cycle 59 (with drift 100 mm) shear force decreased to 470 KN and then, displacement amplitude was decreased and the loading was terminated.

3.2. Elastic and inelastic behavior

Utilizing the experimental results of three specimens under cyclic in-plane loading, the performance of stiffness of each steel shear wall system under monotonic in-plane loading is calculated. The aforementioned stiffness accounted as tangent stiffness is shown in Fig. 12. This figure indicates that the specimen nos. 2 and 3 nearly have similar stiffness performance in the elastic and inelastic range whereas stiffness performance of the specimen no. 1 is somewhat different. The elastic stiffness of the specimen nos. 2 and 3 is nearly 30% larger than that of specimen no. 1. Although an abrupt change in the stiffness does occur at the onset of shear buckling of the corrugated specimens, totally the stiffness of all the specimens is gradually decreased.

Using the cyclic loading results, the elastic and ultimate strength of each steel shear wall system under monotonic loading is calculated. The amount of applied load for occurring the first yielding in the steel shear wall system is nominated as the elastic strength and the maximum applied load is nominated as the ultimate strength. The strength-drift angle relations of all systems are shown in Fig. 13. This figure indicates that elastic strength and the ultimate strength of the tested corrugated specimens are similar and elastic strength of the specimen nos. 2 and 3 is nearly

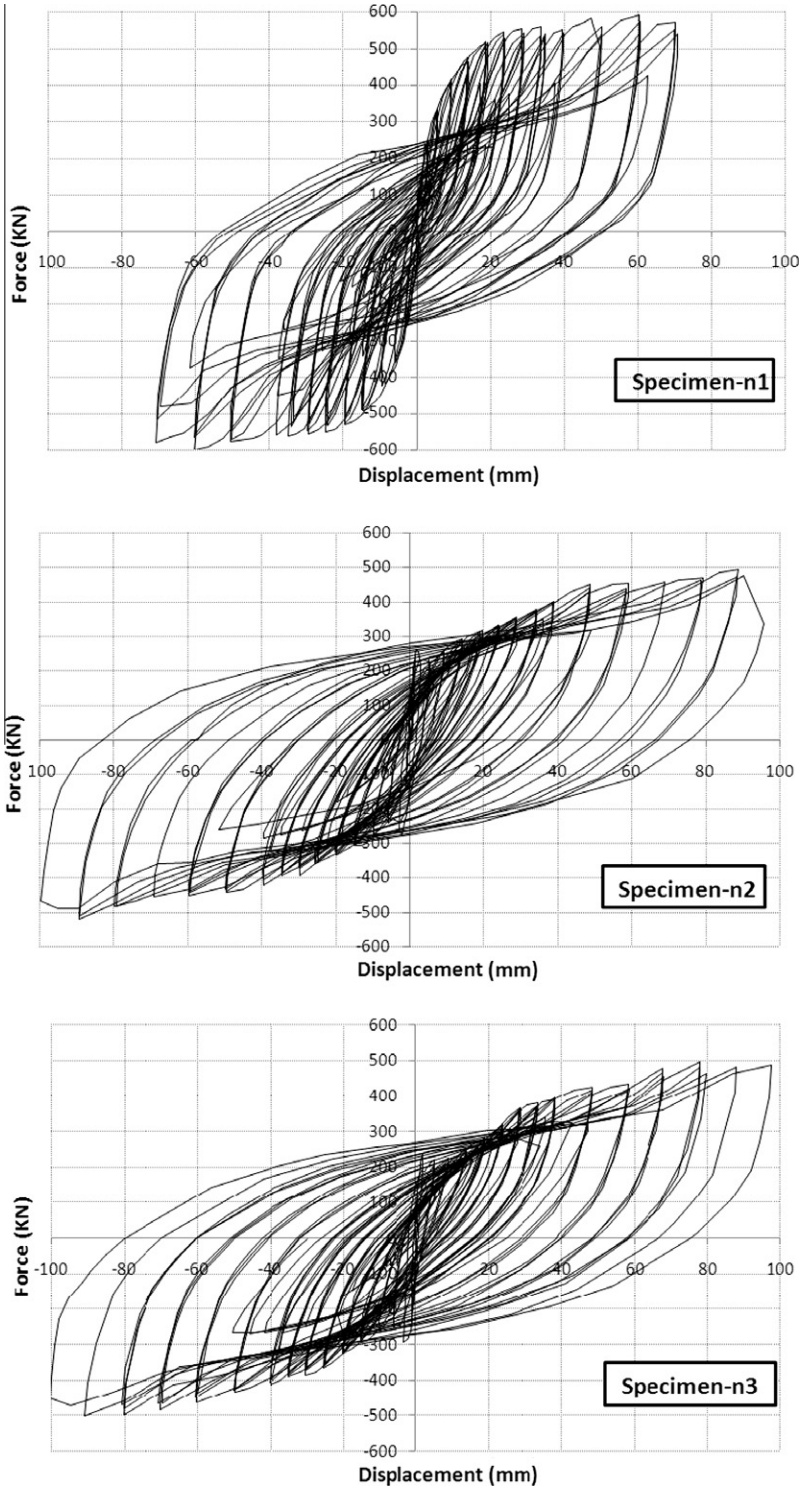

Fig. 10. Hysteresis behavior of the tested specimens.

15% larger compared to the specimen no. 1 whereas the ultimate strength of the specimen no. 1 is about 17% larger than that of the corrugated specimens. It is believed that the lower inelastic strength of the corrugated specimens is due to their accordion behavior. In fact, after inelastic buckling, in-plane stiffness of the corrugated panels decreased abruptly in direction of corrugations. Therefore, the tension field in the corrugated specimens formed incompletely. To design steel plate shear walls, designer should take into consideration to ensure that the steel plate does yield prior to the boundary beams and columns. In fact, the boundary frame is designed to remain elastic as long as it is possible. Thus, by this procedure, the system is able to maintain stability even after the failure of the shear panel. Fig. 14 illustrates the strain-drift angle relations of the panel, column and beam. It is observed that in all the specimens, yielding of the shear panel occurs earlier and with the spreading of plastic zone on the shear panel, the beam end is plastified. At last, the columns can also yield by following the strong column-weak beam design criteria. This arrangement

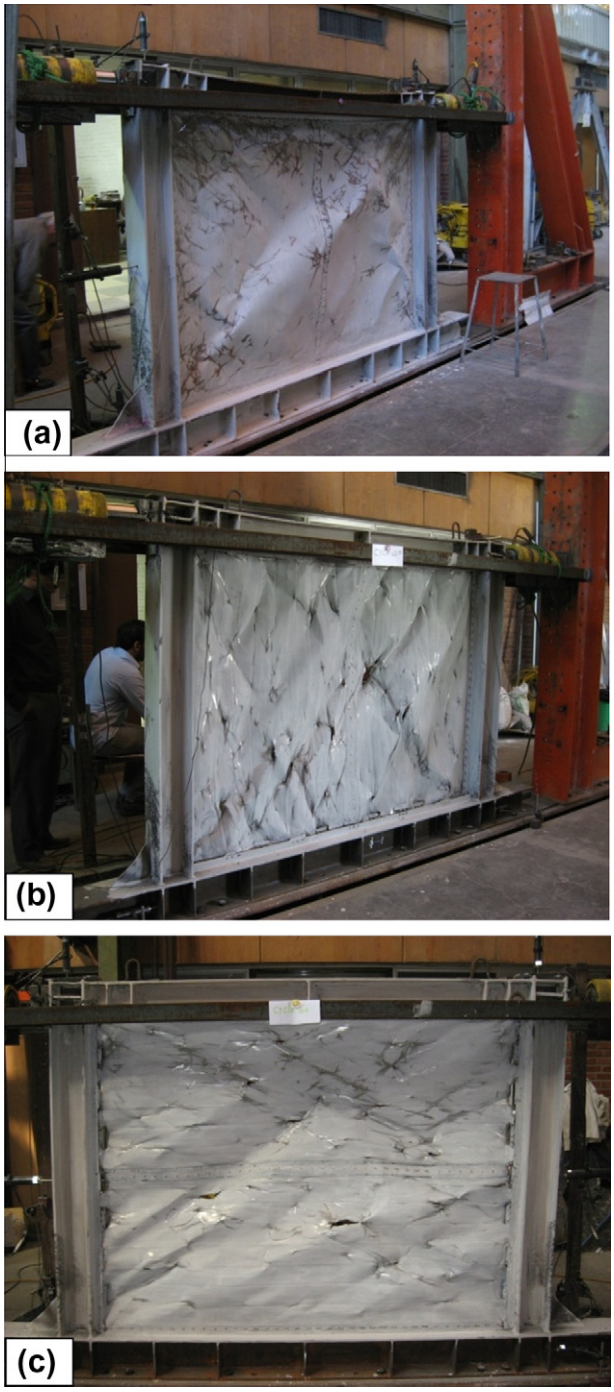

Fig. 11. State of specimens at ultimate stage: (a) specimen no. 1; (b) specimen no. 2; (c) specimen no. 3.

is the capacity design criteria that the steel plate yield before the beam and beam before the columns.

To design the steel shear wall system, it is suggested to permit shear panel yield at moderate earthquake, whereas the boundary frames remain elastically. Under severe earthquake, both the shear panel and the boundary frames are plastified with a large amount of dissipated energy. In this experimental research, unstiffened shear panel and its boundary frames were designed and constructed based on the PFI method. Subsequently, the corrugated specimens were constructed exactly according to the unstiffened specimen only with corrugating steel plates. The experimental results demonstrate that shear wall primarily yields followed with

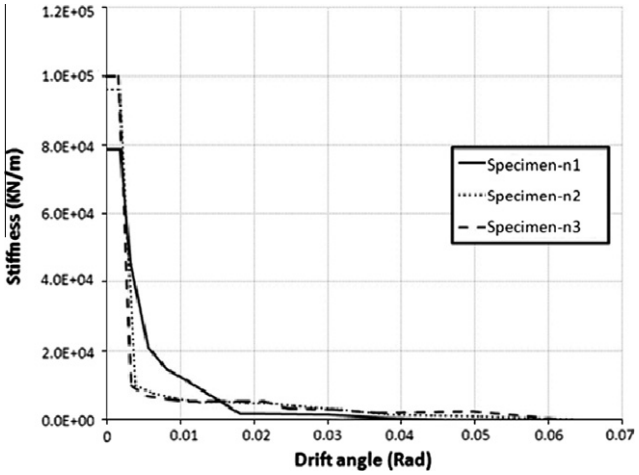

Fig. 12. Stiffness of specimens.

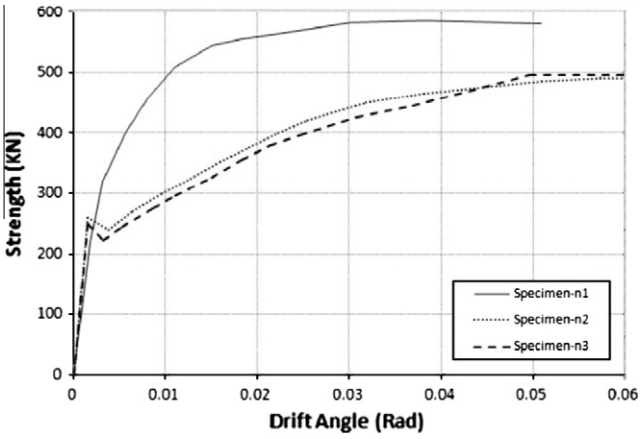

Fig. 13. Strength of specimens under monotonic loading.

the propagation of yielding zone, and eventually the beam and after columns yield near the ultimate state. It is noteworthy that in the corrugated specimens, yielding zone spreads through the entire panel so that at the ultimate state, the number of torn positions in the corrugated panel exceeds about 30 whereas this number reaches 3 in the unstiffened specimen. Therefore, more hysteretic energy dissipates under seismic load. In all specimens, yield of the beam and columns occurs in larger drift angle as shown in Fig. 14. In the unstiffened specimen, it is determined that the beam-to-column connection yields at approximately 0.7% drift angle while the steel panel yields at around 0.16% drift angle. In the corrugated specimens beam-to-column connection yields at approximately 1% drift angle while the corrugated steel panel yields at around 0.12% drift angle.

3.3. Ductility and energy dissipation

Deformability and the amount of energy dissipated under seismic load are major parameters in the lateral load resisting systems. As it was illustrated in Fig. 10, although all the specimens dissipate the energy with stable hysteresis loops, there is pinching in the hysteresis loops of the unstiffened specimen. Both of the corrugated specimens are able to dissipate more energy as oppose to the unstiffened specimen. The cumulated energy at various drift angles is illustrated in Fig. 15. It is perceived that each system can remain elastically prior to 0.2% of drift angle. Furthermore,

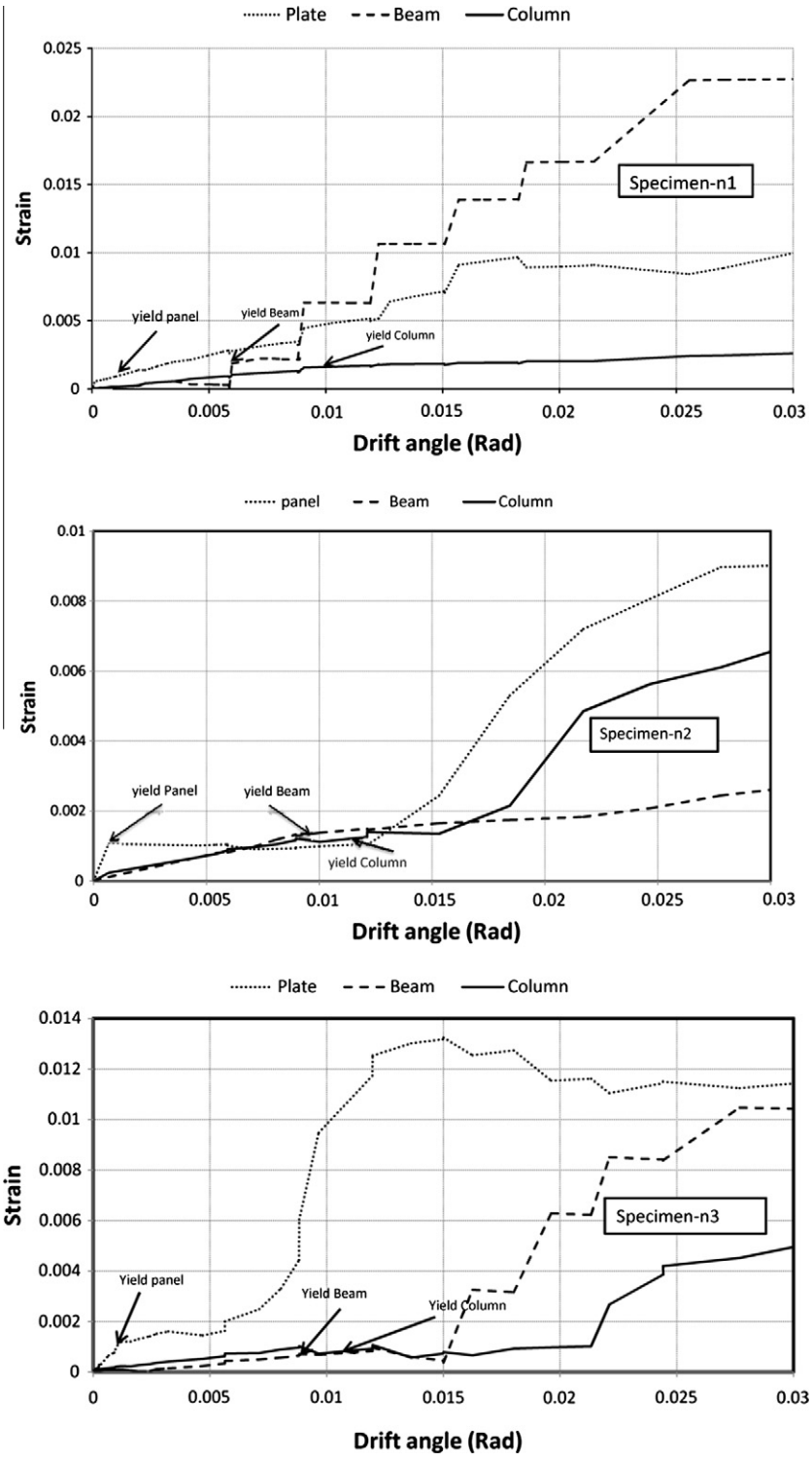

Fig. 14. Inelastic behavior of panel, beam and column.

the specimen nos. 2 and 3 dissipate nearly the same energy in different drift angles. The structural testing of the specimen no. 1 was stopped at 4.5% drift angle due to the decrease of strength whereas the cyclic testing of the specimen nos. 2 and 3 continued up to 6.4% drift angle. Moreover, the total amount of energy dissipated by the specimen no. 1 is about 65% compared to the specimen nos. 2 and 3. Further, it is perceived from the hysteretic curves of the specimens that global behavior of the specimen nos. 2 and 3 is similar to each other but is different with the specimen no. 1. Evidently, the seismic behavior of the corrugated specimens is not affected by changing the direction of corrugations. In addition, although the ultimate strength of the unstiffened specimen is about 17% larger than that of the corrugated specimens, ductility ratio and energy dissipation of the corrugated specimens are approximately 35% and 52% larger than those of the unstiffened specimen, respectively.

According to the performance-based design concept, at the ultimate failure stage, the story drift angle is about 2.5–3% [24,25].

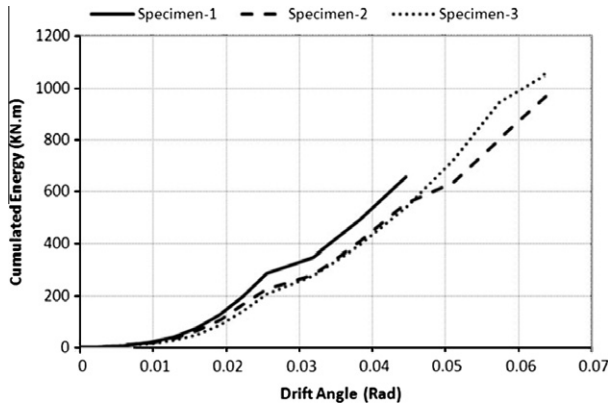

Fig. 15. Cumulated energy of specimens.

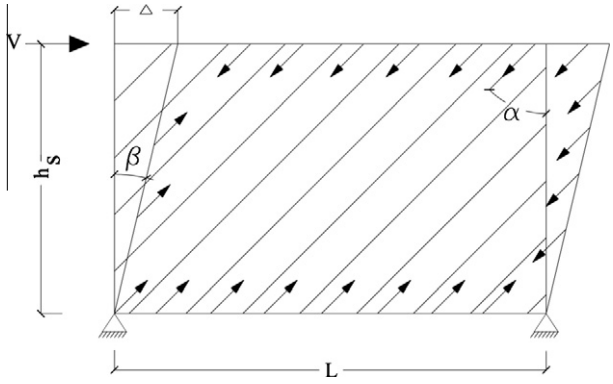

Fig. 16. Single story kinematic collapse mechanism.

Table 3
Summary of test and analytical results (strength and energy).

Specimens	Experimental ultimate strength (KN)	Analytical ultimate strength (KN)		Exp. /Ana. strength		Cumulated energy at 4% drift (KN m)
		Strip model	PFI method	Strip model	PFI method	
No. 1	580	460	518	1.26	1.12	550
No. 2	500	385	487	1.30	1.03	450
No. 3	490	423	540	1.16	0.91	450

Table 4
Summary of test and PFI results (displacement and ductility).

Specimens	Experimental elastic displacement (mm)	Analytical elastic displacement (mm)	Exp./Ana. elastic displacement	Maximum drift angle (Rad)	Ductility ratio
No. 1	3	2.9	1.03	0.04	12
No. 2	3	6.2	0.48	0.06	16
No. 3	3	3.1	0.97	0.06	16

This experimental research demonstrates that by the proper design, the corrugated steel shear walls can achieve 5–7% story drift angle, whereas story drift angle does achieve 3–5% for the unstiffened steel shear walls. Besides, from the hysteretic behavior under quasi-static loading, it is realized that the characteristics of the corrugated steel shear walls are more stable as opposed to the unstiffened steel shear wall.

3.4. Experimental and analytical results

As it was described, the first specimen (specimen no. 1) was designed based on the PFI method [8]. In this section, two methods are employed to analyze all the specimens: plastic analysis of the strip model [26] and Plate-Frame Interaction (PFI). Kinematic method is applied to implement the plastic analysis of the strip model. The same frame is considered with inclined strips instead of the unstiffened steel shear wall with rigid beam-to-column connections as shown in Fig. 16. When the shear force V displaces the top beam by a value Δ sufficient to produce a collapse mechanism, the external work done is equal to $V\Delta$. The internal work done by the yielded strips as well as boundary frame is $(n_b A_{st} F_y \sin\alpha)\Delta + 4M_p\beta$, where n_b and A_{st} are the number and cross-sectional area of the strips anchored to the top beam, respectively. F_y is yield stress of the strips or shear panel. Further, M_p is the smallest of the plastic moment capacity of the beam or columns. Other parameters have been identified in Fig. 16. Using the geometry, $n_b = (L\cos\alpha/s)$, $A_{st} = ts$ and $\beta = \Delta/h_s$, where s is the strip spacing in the direction perpendicular to the strip and t is the thickness of the strips or shear panel. Equating the external and internal work yields:

$$V = (1/2)F_y tL\sin 2\alpha + 4M_p/h_s \tag{9}$$

The shear force of the specimen no. 1 is calculated utilizing Eq. (9). As it was described, in this specimen, the angle of inclination of the principal tension stresses from vertical (α) is approximately 45°. To calculate the shear force of the specimen no. 2, F_y is substituted by the ultimate stress (F_u) in Eq. (9) because of the observed collapse mechanism in the test. Besides, the angle of inclination of the principal tension stresses from vertical (α) determined from the test is 30°. The shear force of the specimen no. 3 is calculated utilizing Eq. (9). For this specimen, the amount of α measured from the tested specimen is 60°.

As it was described in Section 2.1, the specimen no. 1 was designed by the PFI method. To analyze the specimen no. 2 by the PFI method, 0.6L is substituted instead of L in the Eq. (1) because only the flat parts of the corrugated panel were connected to the fish plates located on the beam. Moreover, τ_{cr} is determined based on the interactive shear buckling of the infill corrugated panel due to the observations and information obtained from the kind of the panel buckling. Thus, τ_{cr} is calculated according to the studies implemented by Yi et al. [18] as follows:

$$\tau_{cr} = (1/\tau_{cr,l}) + (1/\tau_{cr,G}) \tag{10}$$

where $\tau_{cr,l}$ is local buckling of the corrugated shear panel when a flat sub-plate between vertical edges buckles and $\tau_{cr,G}$ is global buckling of the corrugated shear panel. $\tau_{cr,l}$ is taken from the classical plate buckling theory by assuming that all the sides of the panels are simply supported and $\tau_{cr,G}$ is calculated from the orthotropic plate buckling theory as following:

$$\tau_{cr,l} = [5.34 + 4(a/h_s)^2]\pi^2 E/[12(1-\nu^2)(a/t)^2] \tag{11}$$

$$\tau_{cr,G} = 36\beta E\{[(d/t)^2 + 1]/6\eta\}^{3/4}(t/h_s)^2/[12(1-\nu^2)]^{1/4} \tag{12}$$

where a is flat panel width; E and ν are Young's modulus of elasticity and Poisson's ratio, 210 GPa and 0.3, respectively. The coefficient β is assumed 1.0 according to the boundary conditions of the shear panel and $\eta = (a+b)/(a+c)$.

The parameters b and c are horizontal projection of the inclined panel width and inclined panel width, 86.6 and 100 mm, respectively. To account for the effects of inelasticity, residual stress and initial deformations Eq. (13) proposed in the Design Manual [24] is applied.

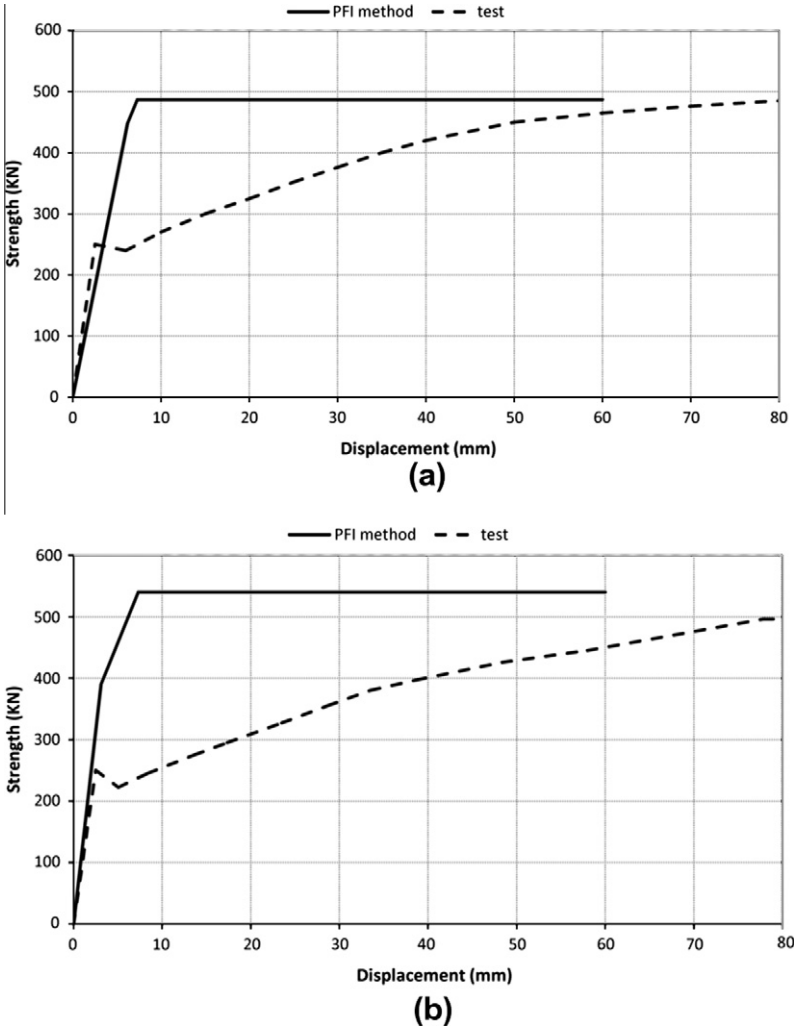

Fig. 17. Experimental and analytical Strength: (a) Specimen no. 2; (b) Specimen no. 3.

$$\frac{\tau_{cr}}{\tau_y} = \begin{cases} 1 & \lambda_s < 0.6 \\ 1 - 0.614(\lambda_s - 0.6) & 0.6 < \lambda_s \leqslant \sqrt{2} \\ 1/\lambda_s^2 & \sqrt{2} < \lambda_s \end{cases} \quad (13)$$

where $\lambda_s = (\tau_y/\tau_{cr})^{0.5}$. Finally, the ultimate strength of this corrugated specimen is calculated by the sum of the modified Eqs. (1) and (5).

The limiting shear elastic displacement of the frame of this specimen (U_{fe}) is determined by applying Eq. (6) and the limiting shear elastic displacement of its corrugated panel (U_{we}) is calculated as following:

$$U_{we} = U_{wcr} + U_{wpb} = (\tau_{cr}/G + 3.5\sigma_{ty}/E \sin 2\theta)h_s \quad (14)$$

U_{wcr} is shear buckling displacement of the corrugated panel and U_{wpb} is shear displacement of the corrugated panel due to the configuration of the tension field. The U_{wpb} is calculated with the conception of equality of work done by shear stresses and strain energy.

To analyze the specimen no. 3 by the PFI method, similar to the specimen no. 2, τ_{cr} is calculated according to the studies implemented by Yi et al. [18]. Finally, the ultimate strength of this corrugated specimen is calculated by adding Eqs. (1) and (5). Furthermore, the limiting shear elastic displacement of the frame of this specimen (U_{fe}) is determined by applying Eq. (6) and the shear displacement of the corrugated panel due to the configuration of the tension field (U_{wpb}) is calculated based on the conception of equality of work done by shear stresses and strain energy. Then, the limiting shear elastic displacement of its corrugated panel (U_{we}) is determined as following:

$$U_{we} = U_{wcr} + U_{wpb} = (\tau_{cr}/G + 2.14\sigma_{ty}/E \sin 2\theta)h_s \quad (15)$$

The comparisons of the analytical results from the plastic analysis of the strip model as well as the PFI method with experimental study are shown in Tables 3 and 4. It is determined that the PFI method can predict the ultimate strength of the corrugated specimens with fairly reasonable accuracy. Besides, strength–displacement relations of the corrugated specimens determined by the test and PFI method are compared in Fig. 17. It is perceived that although the initial stiffness of the corrugated specimens as well as their ultimate strength obtained by the test and PFI method are coincident, the limiting shear elastic displacement of the corrugated panels should be modified. Thus, buckling and postbuckling behavior of the corrugated shear panels of these specimens need to be more accurately investigated.

4. Conclusions

The corrugated steel plate carries high out-of-plane stiffness and high elastic shear strength. By the proper design of the

corrugated steel shear wall, the corrugated steel plate is able to yield at predetermined force level and dissipate the seismic energy through plastic deformation without any pinching in the hysteretic loops. Besides, due to the accordion effect of the corrugated panels, deformability and ductility ratio of the corrugated steel shear wall system is very large. Although further studies are definitely required to be carried out, based on the present research, the ultimate story drift angle can be as large as 5–7% in this system.

Furthermore, the experimental results reveal that under similar condition such as boundary frames, beam-to-column connections and plate thickness, both of the corrugated and unstiffened steel shear walls primarily yield and then the beam-to-column connection yields with the propagation of yielding zone. It is noteworthy that in the corrugated specimens, yielding zone propagates nearly the entire corrugated panels whereas such phenomenon is not observed in the unstiffened specimen. Moreover, the experimental study indicates that the total energy dissipation of the corrugated specimens is approximately 1.52 times higher than that of the unstiffened specimen. Although further research is necessary, it is tentatively suggested that by studying the buckling and post-buckling behavior of the corrugated shear panels more comprehensively, the PFI method can be utilized for the proper design of the corrugated steel shear walls as well as the unstiffened shear walls.

Acknowledgments

This research work was supported by the Building & House Research Center (BHRC) of Iran. Their support is acknowledged with thanks.

References

[1] Driver RG, Kulak GL, Kennedy DJL, Elwi AE. Cyclic test of four-story steel plate shear wall. J Struct Eng ASCE 1998;124(2):112–20.
[2] Caccese V, Elgaaly M, Chen R. Experimental study of thin steel-plate shear walls under cyclic load. J Struct Eng ASCE 1991;119(2):573–88.
[3] Berman JW, Celik QC, Bruneau M. Comparing hysteretic behavior of light-gauge steel plate shear walls and braced frames. Eng Struct 2005;27(3):475–85.
[4] Topkaya C, Kurban CO. Natural periods of steel plate shear wall systems original research article. J Construct Steel Res 2009;65(3):542–51.
[5] Berman JW. Seismic behavior of code designed steel plate shear walls. Eng Struct 2011;33(1):230–44.
[6] Roberts TM. Seismic resistance of steel plate shear walls. Eng Struct 1995;17(5):344–51.
[7] Bhowmick AK, Driver RG, Grondin GY. Seismic analysis of steel plate shear walls considering strain rate and P-delta effect. J Construct Steel Res 2009;65(5):1149–59.
[8] Sabouri-Ghomi S, Ventura CE, Kharrazi MHK. Shear analysis and design of ductile steel plate walls. J Struct Eng ASCE 2005;131(6):878–89.
[9] Bhowmick AK, Grondin GY, Driver RG. Estimating fundamental periods of steel plate shear walls. Eng Struct 2011;33(6):1883–93.
[10] Liu S, Warn GP. Seismic performance and sensitivity of floor isolation systems in steel plate shear wall structures. Eng Struct 2012;42:115–26.
[11] Qu B, Guo X, Chi H, Pollino M. Probabilistic evaluation of effect of column stiffness on seismic performance of steel plate shear walls. Eng Struct 2012;43:169–79.
[12] Takahashi Y, Takemoto Y, Takeda T, Takagi M. Experimental study on thin steel shear walls and particular bracings under alternative horizontal load. Preliminary rep. IABSE symp. on resistance and ultimate deformability of struct. Acted on by well-defined reported loads. International Association for Bridge and Structural Engineering, Lisbon, Portugal; 1973, pp. 185–191.
[13] Thorburn LJ, Kulak GL, Montgomery CJ. Analysis of steel plate shear wall. Structural engineering report no. 107. Canada: University of Alberta; 1983.
[14] Easley JT, McFarland DE. Buckling of light-gauge corrugated metal shear diaphragms. J Struct Div ASCE 1969;95:1497–516.
[15] Elgaaly M, Hamilton RW, Seshadri A. Shear strength of beam with corrugated webs. J Struct Eng ASCE 1996;122(4):390–8.
[16] Ibrahim SA, El-Dakhakhni VW, Elgaaly M. Behavior of bridge girders with corrugated webs under monotonic and cyclic loading. Eng Struct 2006;28(14):1941–55.
[17] Sayed-Ahmed EY. Behavior of steel and (or) composite girders with corrugated steel webs. Can J Civ Eng 2001;28:656–72.
[18] Yi J, Gil H, Youm K, Lee H. Interactive shear buckling corrugated steel webs. Eng Struct 2008;30(6):1659–66.
[19] AC 154. Acceptance criteria for cyclic racking shear tests for metal-sheathed shear walls with steel framing. ICC Evaluation Service, INC; 2008.
[20] ASTM E8M-04. A 370-06 Standard test methods and definitions for mechanical testing of steel products; 2006.
[21] DIN 1623. 1629 International Standard of Germany; 1983.
[22] ANSI/AWS D1.1-98. Structural welding code-steel. American Welding Society; 1998.
[23] ATC-24. Guidelines for cyclic testing of components of steel structures. Stanford (California): Stanford University; 1992.
[24] FEMA. NEHRP guidelines for the seismic rehabilitation of buildings. FEMA-273. Washington, DC: Federal Emergency Management Agency; 1997.
[25] SEAC. Performance based seismic engineering of buildings. Vol. 1, Structural Engineering Association of California; 1995.
[26] Berman J, Bruneau M. Plastic analysis and design of steel plate shear walls. J Struct Eng ASCE 2003;129(11):1448–54.